Learning Fingertip Force to Grasp Deformable Objects for Soft Wearable Robotic Glove With TSM

Eojin Rho, Daekyum Kim, Hochang Lee, and Sungho Jo, *Senior Member, IEEE*

***Abstract*—Soft wearable robotic gloves based on tendon-sheath mechanism are widely developed for assisting people with a loss of hand mobility. For these robots, knowing the fingertip forces applied to deformable objects is crucial in successfully grasping them without causing excessive deformations. Existing studies presented methods to predict fingertip force applied to rigid objects only using information from the actuation system. However, forces applied to deformable objects are subject to non-linearity and hysteresis in relation to the objects' stiffness, which further complicates the problem. Therefore, this letter proposes a deep-learning model that can accurately estimate the fingertip forces applied to deformable objects using motor encoder values, motor current, and wire tension. Our model is based on an integrated system of Long Short-Term Memory models that 1) estimates stiffness of the grasped objects and 2) incorporates the estimated stiffness for predicting the fingertip forces. When evaluated using a TSM-based soft wearable robot, the proposed model recorded fingertip force estimation of 0.702 N RMSE, achieving 45% increase in accuracy compared to LSTM that does not consider the objects' stiffness. The applicability of our method was evaluated by estimating the fingertip forces applied to common daily items and performing real-time force control.**

***Index Terms*—Soft robot applications, wearable robotics, deep learning methods, modeling, control and learning for soft robots.**

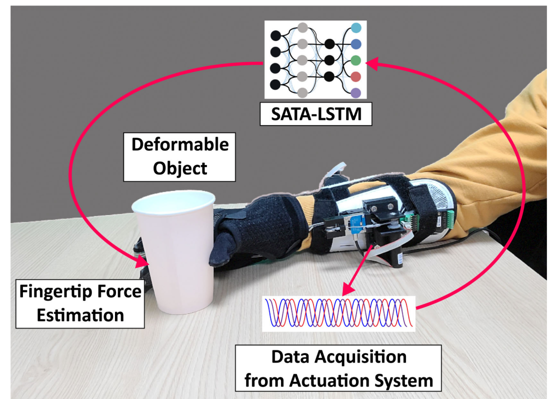

Fig. 1. System overview. Deformable objects are grasped using the tendon-driven soft wearable robotic glove system developed for the study. The applied fingertip forces are predicted using the SATA-LSTM algorithm proposed in the letter.

I. Introduction

SOFT wearable robotic gloves driven by Tendon-Sheath Mechanisms (TSM) have been recently developed to assist users with a loss of hand mobility [1]–[9]. The tendon-driven systems, which generally comprise a glove, an actuation system, and a TSM, include the following common features: 1) Reduced weight of the end-effector due to the separation between the actuation system and the glove, 2) Under-actuation of the glove, which limits the degree of freedom to employ a fewer number of actuators, thus reducing the system's complexity [3].

For users to grasp objects of various physical properties, the wearable robots must be capable of applying the appropriate amount of force to the objects. This is especially important when grasping deformable objects like a thin letter cup. For example, consider a case in which a user wearing the robotic glove tries to hold a flexible takeout cup filled with coffee. Without the proper control of fingertip forces applied to the cup, the robotic glove can deform the cup to a point that causes spillage of the contained liquid. Therefore, knowing the forces generated at the fingertips is a key factor in successful object-grasping.

For systems employing TSM, recent studies have attempted to measure forces at the distal-ends by using information from the proximal-ends [10]. This approach has advantages applicable for wearable robotic gloves compared to placing sensors on the glove such that 1) it eliminates the need for individual calibration and 2) the absence of external sensor-related electronics makes the glove less bulky and robust against watery environments [10], [11]. However, the non-linear relationships among the data collected from the actuation system along with discrepancies in force profiles during loading and unloading, known as hysteresis, cause difficulties in predicting the applied forces. Recently, deep learning-based methods have been used to address these issues [10], [12]. Li *et al.* proposed to predict the hysteresis of TSM in the endoscopic device under quasi-static environments. Kang *et al.* proposed a learning-based method to estimate fingertip forces under dynamic movements of TSM. However, there is a lack of studies that attempt to estimate the forces applied to objects of varying degrees of deformation using wearable robotic gloves that are not equipped with external sensors.

Manuscript received February 23, 2021; accepted July 18, 2021. Date of publication August 6, 2021; date of current version August 25, 2021. This letter was recommended for publication by Associate Editor L. Beccai and Editor C. Laschi upon evaluation of the reviewers' comments. This work was supported by the National Research Foundation of Korea Grant funded by the Korean Government (MSIT) under Grant NRF-2016R1A5A1938472. *(Eojin Rho and Daekyum Kim contributed equally to this work.) (Corresponding author: Sungho Jo.)*

The authors are with the School of Computing, KAIST, Daejeon 34141, South Korea (e-mail: djwls9453@kaist.ac.kr; daekyum@kaist.ac.kr; hochang.lee91@kaist.ac.kr; shjo@kaist.ac.kr).

This letter has supplementary downloadable material available at https://doi.org/10.1109/LRA.2021.3102968, provided by the authors.

Digital Object Identifier 10.1109/LRA.2021.3102968

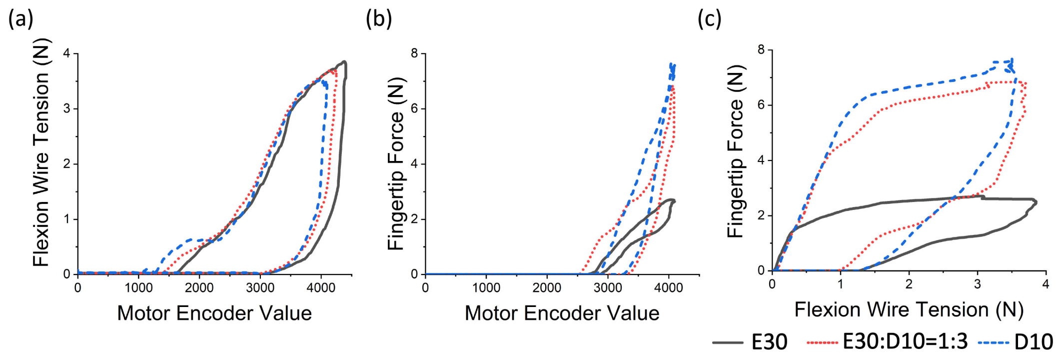

Fig. 2. Non-linear patterns among flexion wire tension, flexion motor encoder value, and fingertip force when grasping objects of varying stiffness: Ecoflex-0030 (E30), 1:3 Mixture of Ecoflex-0030 and Dragonskin 10 (E30:D10=1:3), and Dragonskin 10 (D10), listed in the order of increasing stiffness (a) Motor encoder value vs. Flexion wire tension (b) Motor encoder value vs. Fingertip force (c) Flexion wire tension vs. Fingertip force.

It is known that the non-linearity of TSM, wearable glove, and user's hand impedes accurate estimation of fingertip forces [10], [13]. In addition to this, the stiffness of deformable objects can bring about varying non-linearity patterns, which causes difficulties when measuring fingertip forces. Despite being deformed to a similar degree, the forces applied to the objects can significantly differ depending on the objects' stress-strain relationship. Thus, without considering object stiffness information, it is difficult to estimate fingertip forces applied to objects with varying degrees of deformability.

In this study, we propose a learning-based model that estimates fingertip forces applied to deformable objects by using motor encoder values, motor currents, and wire tensions for TSM-based soft wearable robotic gloves. Assuming that objects' stiffness is a dominant mechanical property for deformation, this approach can be used to estimate the fingertip forces applied to objects of varying deformability. Previous study [10] proposed the learning-based approach to estimating fingertip forces applied to rigid objects, using motor encoder values, wire tensions, and sheath bending angles. In contrast, our method not only estimates the forces applied to rigid objects, but incorporates objects' estimated stiffness to predict the forces applied to deformable objects. In order to realize this, a tendon-actuation based wearable robotic glove equipped with an forearm-wearable actuation system was designed. This system not only increased the robot's portability, but minimized the changes in sheath-bending angle, which was a significant factor effecting the applied fingertip forces [10]. To successfully estimate the applied fingertip forces, our research proposes Stiffness-Aware Temporal-Attention Long Short-Term Memory (SATA-LSTM). LSTM [14] models have been utilized in various areas of soft robotics, such as calibration of soft sensors [15] and modeling the kinematics of soft pneumatic actuators [16], because of their high performances in training time-dependent data to capture non-linearity and hysteresis of a system. Using the LSTM model, SATA-LSTM comprises two main components: the stiffness estimation model and the fingertip force estimation model. First, the grasped object's stiffness is estimated using a LSTM model trained on data from the actuation system. Then, the stiffness information is continuously updated to the inputs and hidden layers of the fingertip force estimation model. Finally, the LSTM's hidden layer output, which contains actuation system data and stiffness information, is enhanced through temporal attention. By employing the proposed architecture, SATA-LSTM can accurately estimate the change in fingertip forces caused by the object's stiffness.

The performance of SATA-LSTM was compared against the existing learning-based approaches and our prototype, an LSTM model that includes the estimated stiffness only as part of its initial input. We also evaluated the performance of stiffness estimation model for objects of varying stiffness. To test our model's real-world applicability, we compared the performances in force estimation errors and the computation times for various sequence time lengths of input data. Moreover, we compared the performances of various models in regards to the object yielding least accurate fingertip force estimations. Finally, we tested our model's applicability by estimating the fingertip forces applied to untrained objects found in daily life. Then we evaluated our model's repeatability on a reassembled system, and performed real-time force control on objects of different stiffness.

II. Problem Regarding Stiffness

This section emphasizes the non-linear relationships caused by objects' varying stiffness. Fig. 2(a)–(c) shows the non-linear relationships between fingertip forces and other parameters for three deformable objects : Ecoflex-0030, 1:3 Mixture of Ecoflex-0030 and Dragonskin 10, and Dragonskin 10 (567 N/m, 1433 N/m, 1967 N/m). Fig. 2(a) shows that as the stiffness of the grasped object decreases, both the flexion motor encoder values and the flexion wire tension increase. Fig. 2(b) shows the relationship between the flexion motor encoder values and fingertip forces. The lower the object's stiffness, the more deformation occurs, subsequently causing greater changes in motor encoder values. On the contrary, higher fingertip forces are measured for objects of higher stiffness. This shows that greater amount of force is required to deform objects with higher stiffness compared to objects with lower stiffness. In Fig. 2(c), the decrease in stiffness causes a decrease in fingertip forces measured, but incurs higher flexion wire tension. The relationships among encoder values, flexion wire tension, and

Fig. 3. Overview of TSM-based soft wearable robotic glove and stiffness measuring apparatus (a) Neuro-Augmented Machine-Enhanced Tendon-driven Assistive Glove (NAME-TAG) (b) Actuation system (c) Stiffness measuring apparatus and cylindrical objects used for data collection.

fingertip forces display differing trends depending on the objects' stiffness. It can be noted that the non-linearity among these parameters and hysteresis are subject to change depending on the objects' stiffness. Based on this, it can be concluded that fingertip forces can greatly vary depending on objects' stiffness, making the force estimation difficult.

III. Methods

A. Hardware Setup

1) *Wearable Robotic Glove:* We developed a wearable robotic glove system named Neuro-Augmented Machine-Enhanced Tendon-driven Assistive Glove (NAME-TAG). It is a wearable robotic glove featuring an actuation system that can be worn at the forearm connected to the glove via TSM (Fig. 3). The glove made from flexible polyamide material was fitted with rings located near the joints of the phalanges to pass the force-transferring wires through. The rings were selectively placed near the metacarpophalangeal (MCP), proximal interphalangeal (PIP), and distal interphalangeal (DIP) joints to mimic flexion tendons passing through the joints in a human hand [9], [17]. This design enables to manipulate the glove into grasping and releasing motions. The flexion tendons were wired at the palm of the hand while the extension tendons were routed at the back of the hand. These wires would be pulled and released antagonistically to form grasping and releasing motion of the glove.

In order to perform stable grasping of objects, the thumb must support the objects to prevent them from sliding. Therefore, we employed a thumbguard (Thumb Guard Soft, ZAMST, Japan) to prevent the thumb from bending backwards during the grasping

TABLE I
Deformable Object Information

Object	Material	Stiffness (mean±std N/m)
O1	Ecoflex-0030	567±17
O2	Ecoflex-0050	683±15
O3	1:1 (Ecoflex-0030 : Dragonskin 10)	950±19
O4	1:3 (Ecoflex-0030 : Dragonskin 10)	1433±33
O5	1:6 (Ecoflex-0030 : Dragonskin 10)	1733±21
O6	Dragonskin 10	1967±15
O7	3D-Printed (PLA)	Rigid

of objects. This ensured that the object remained within glove and that the applied forces could be measured accurately.

The actuation system consisted an assembly of DC motors (1524 A 012SR, FAULHABER, Germany) and loadcells (DBSM-10, Bongshin, S. Korea) that was mounted on two shin guards (Super light shing guards, Franklin, USA) to be worn at the forearm. The DC motors located at the opposite sides of the forearm worked antagonistically to form grasping and releasing of the glove. In order to grasp an object, the motor located at the bottom of the forearm would pull the flexion wire while the opposite motor would release the extension wire; for releasing an object the motors would operate vice versa. The loadcells were fixed in front of the motor, such that they could measure the tension in the wires during the grasping of various objects.

TSM that connected the actuation system to the glove remained fixed in order to reduce the effects of dynamic changes in sheath bending angles. The sheaths were slightly stretched to maintain a tight, straight connection between supporting pieces located at the palm of the glove and the actuation system. This design minimized the bending of the sheath during operation, preventing the increase in contact between the wires and the sheath. Additionally, the change in fingertip force caused by dynamic changes in sheath bending angle [10] were effectively minimized.

2) *Deformable Objects:* In order to obtain various measurable stiffness values of deformable objects, we created deformable cylinders from silicone mixtures (Ecoflex and Dragonskin, Smooth-On, USA). The 5 cm by 10 cm (diameter × height) mold was 3D-printed (Single Plus, Cubicon, S. Korea) into two open parts, and silicone mixtures were injected into the closed mold. Prior to being poured into the mold, each silicone mixture was placed in a vacuum chamber (1HP Vacuum Pump, Hyup-Shin, S. Korea) to remove the air bubbles to prevent cylinders from tearing. Then, the mixtures were baked in a convection oven (WOF07105, Daihan Scientific, S. Korea) at 60 °C for 35 to 40 minutes and cooled at room temperature for 5 minutes before being removed from the mold [18]. Lastly, a cylinder of same size, 3D-printed using PLA, was chosen as the rigid object for our experiment.

B. Data Collection

1) *Stiffness Measuring:* The stiffness of the cylinderical objects made from silicone mixtures were measured 10 times for

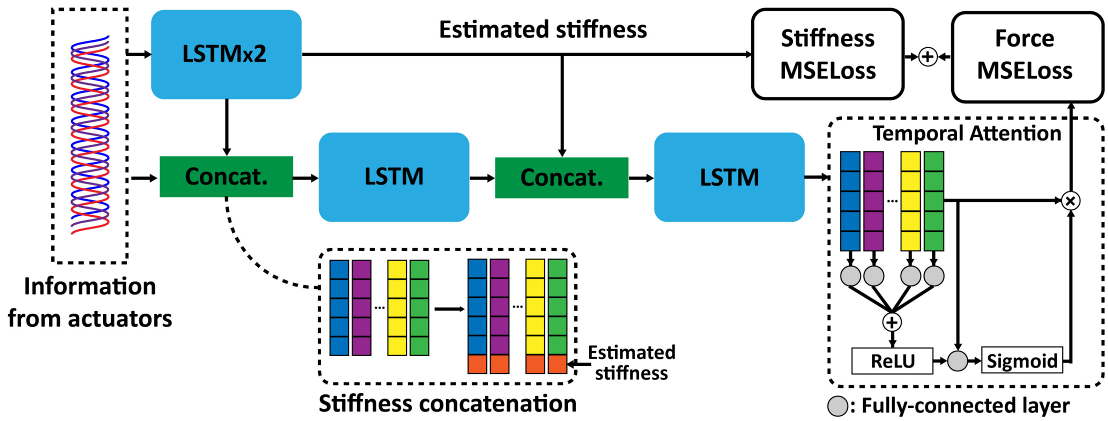

Fig. 4. Stiffness-Aware Temporal-Attention Long Short-Term Memory (SATA-LSTM).

each object using a force sensor mounted on a CNC milling machine (MiniMill, OpenBuilds, USA). A 3D-printed PLA piece with a 1.2 mm tip, covered in soft silicone, was attached to the bottom of the force sensor. This was done to imitate the contact between the grasped object and the fingertip when using the wearable robotic glove robot. The deformable objects were pressed in stiffness-measuring assembly until incurring 6 mm deformation. Then, the measured forces were divided by the amount of deformation to obtain the stiffness of each object. Table I shows the list of cylindrical objects used in our experiment along with their stiffness and mixing ratios.

2) *Data Collection:* During the experiment, a user wearing the robotic glove remained seated and maintained relaxed hand posture. The wearable robotic glove was set to an open-hand position and the encoder values of the flexion and extension motors were initialized. For each trial, the flexion motor was commanded to pull the flexion wire, wrapped around a spool 1 cm in diameter, about 9.4 cm to firmly grasp each object. During this, the extension motor was commanded to slightly release the extension wire to reduce the tension at the back of the hand. In order to release the object, the flexion motor and extension motor were both commanded to return to their original position. This method of operation allowed for firm grasping and full extension of the glove during the experiment. FSR (FSR 402, Interlink, USA) sensor was attached at the tip of index finger to measure the forces applied to the objects during grasping. To improve the sensor performance, 1 mm thick disks made of PLA were attached at the back and the front of the FSR sensor [19]. This modification prevented the sensor from deforming and evenly distribute the force applied to it, increasing the measurement accuracy. 7 cylinderical objects in total, 6 deformable and 1 rigid, were grasped using the wearable robotic glove. These objects had stiffness values ranging from 567 N/m to 1967 N/m for the 6 deformable objects. Each object was grasped-and-released 100 times and data were sampled at 100 Hz. 80 trials for each object were used for training and validation, and 20 trials were used for testing. The collected data was used to train the models, including our SATA-LSTM, described in the following section.

TABLE II
INPUT DATA

Index	Variable	Label
1	x_t^1	Tension value of extension wire (middle finger)
2	x_t^2	Tension value of extension wire (index finger)
3	x_t^3	Tension value of flexion wire
4	x_t^4	Motor encoder value
5	x_t^5	Motor current
6	x_t^6	Difference of motor encoder value in time
7	x_t^7	Difference of motor current value in time

C. Algorithm

In order to obtain the applied fingertip forces from the sequential input data, we have developed our fingertip force estimation model based on Long Short-Term Memory (LSTM), which is a variant of Recurrent Neural Network (RNN). By incorporating input, forget, and output gates the LSTM algorithm display improved performances in dealing with long range dependencies, which is often difficult due to exploding and vanishing gradients [20]. However, LSTM models need to be further modified to consider the objects' stiffness as the fingertip forces applied to deformable objects largely depend on objects' stiffness. In this study, we propose Stiffness-Aware Temporal-Attention LSTM (SATA-LSTM) that utilizes information about object's stiffness to accurately predict the fingertip forces applied to deformable objects.

1) *Input/Output Data:* The input data has a sequence time window T, and input value of x_t at each time step t. At time $t = 1, 2, \ldots, T$, we define $x_t = \{x_t^1, x_t^2, \ldots, x_t^7\}$, where each variable is shown in Table II. The collection of sensor inputs for the sequence time window T is represented as $x_{1:T}$. For the output data, s_T and y_T represent the stiffness and the fingertip force at time T.

2) *SATA-LSTM:* The SATA-LSTM model, shown in Fig. 4, is composed of two main parts: the stiffness estimation model and the force estimation model. The estimated stiffness s_T is concatenated with the LSTM input $x_{1:T}$ and hidden layer features $H_{1:T}$ to form $\hat{x}_{1:T}$ and $\hat{H}_{1:T}$, which contains the updated information about the object stiffness. Adding the stiffness information to all input and hidden layers prevents the force estimation model from improperly reflecting the object's stiffness due to

gradient vanishing. The force estimation model is composed of two LSTM layers that retain information of object stiffness and a temporal attention network. Our attention mechanism utilizes fully-connected layers and subsequent activation functions to aggregate the information from each time step within the input sequence [21]. Through this process, which we call Temporal Attention [21], [22], our model focuses on important temporal features of the data. $\hat{H}_{1:T}$, the input of temporal attention, contains knowledge of the data from actuation system updated with information about objects' stiffness. By integrating this information we created the following query feature in which W and b are trainable parameters and $ReLU(\bullet)$ is a rectifier linear unit activation function.

$$q_T = ReLU\left(\sum_{t=1}^{T} W\hat{H}_t + b\right) \tag{1}$$

Then, attention for each time step is calculated as the following.

$$\alpha_T = Sig(W_h\hat{H}_T + W_q q_T + b_h + b_q) \tag{2}$$

Here, W_h, W_q, b_h, b_q are trainable parameters, and $Sig(\bullet)$ is a sigmoid activation function to obtain a probability between 0 and 1. After applying attention, the hidden state feature is represented as $(1 + \alpha_T) \cdot \hat{H}_T$. Then, the attention-enhanced hidden state feature is fed to the fully connected layer to estimate the fingertip forces. The SATA-LSTM trains the stiffness estimation model and the force estimation model simultaneously. Therefore, the loss function is defined as the sum of the two models' Mean Squared Error loss, which is represented as the following,

$$L = \frac{1}{N}\sum_{i=1}^{N}(y_i - \hat{y}_i)^2 + \frac{1}{N}\sum_{i=1}^{N}(s_i - \hat{s}_i)^2 \tag{3}$$

where $\hat{y}_i$ and $\hat{s}_i$ represent ground truth force and ground truth stiffness information, respectively. N represents the number of input data in each batch.

3) *Implementation Details:* The SATA-LSTM proposed in this letter utilizes two-layered LSTM with a hidden-layer size of 100 to estimate applied fingertip forces. The stiffness estimation model is also composed of two layers of LSTM with 100 hidden units. The sequence time length of each LSTM is T = 40. The stiffness estimation and temporal attention are respectively followed by fully connected layers to produce one-dimensional outputs. The output sizes of the fully connected layers in temporal attention are fixed at 10. The training epoch is 500 with a batch size of 32. Adam optimizer with 0.001 learning rate and weight decay of 10^{-5} is used.

IV. Results

The performance of SATA-LSTM was evaluated by comparing it against five different learning-based models, which included linear regression (LR), random forest regression (RF), a model composed of 3 fully connected layers (FC), 2-layered LSTM [14] model (LSTM), and LSTM model in which the estimated stiffness is appended to the initial input data (LSTM+Stiffness). The performance of each model was evaluated using Root Mean Squared Error (RMSE), Mean Absolute Error (MAE), and Mean Absolute Percentage Error (MAPE).

TABLE III
Fingertip Force Estimation Results

	RMSE (N)	*MAE* (N)	*MAPE* (%)
LR	1.626	1.266	31.3
RF	1.403	1.025	24.8
FC	1.426	0.920	19.1
LSTM	1.049	0.691	18.1
LSTM+Stiffness	0.827	0.538	13.2
Ours	**0.702**	**0.462**	**11.3**

A. Fingertip Force Estimation

The results of testing data set for various models are summarized in Table III. The LR model resulted in RMSE of 1.626 N and MAE of 1.266 N. RF model showed 1.403 N RMSE and 1.025 N MAE. The FC model performed at RMSE of 1.426 N and MAE of 0.920 N. In the case of LSTM, an improved performance of 1.049 N RMSE and 0.691 N MAE were recorded. LSTM+Stiffness model yielded RMSE of 0.827 N and MAE of 0.538 N. Our proposed model, SATA-LSTM, achieved the best results of 0.702 N RMSE and 0.462 N MAE.

The LR, RF, and FC models displayed significant errors because they could not consider the temporal characteristics of the input data. While the LSTM model displayed improved performance over the aforementioned models, it still could not accurately predict the fingertip forces. Despite learning the temporal dependencies of the input data, LSTM model failed to consider the effects of object deformation. To resolve this issue, we proposed to estimate objects' stiffness using the data from the actuation system. The LSTM+Stiffness model, which utilizes objects' estimated stiffness as an input, had 26.8% RMSE and 28.4% MAE improvements compared to LSTM. Our final model, SATA-LSTM, further increased the performance by reflecting objects' stiffness to each LSTM layer and implementing temporal attention. This translated to 49.4% RMSE and 49.6% MAE improvements compared to the LSTM without stiffness information. The fingertip force estimation results for three deformable objects of varying stiffness and a rigid object, using three different algorithms, are depicted in Fig. 5.

B. Stiffness Estimation Performance

Integration of object stiffness with the input features is a key factor in accurately estimating the fingertip forces applied to deformable objects. For its best predictions, stiffness estimation model achieved the least error for O1 (567 N/m) with RMSE of 14.89 N/m and yielded the most error for O6 (950 N/m) with RMSE of 67.368 N/m. It is presumed that object O6 dataset included many data points that resembled the data related to object of similar stiffness, which decreased stiffness prediction performance. Despite the variance for some objects, it can be noted that our model could predict the objects' stiffness within the 7.1% error margin.

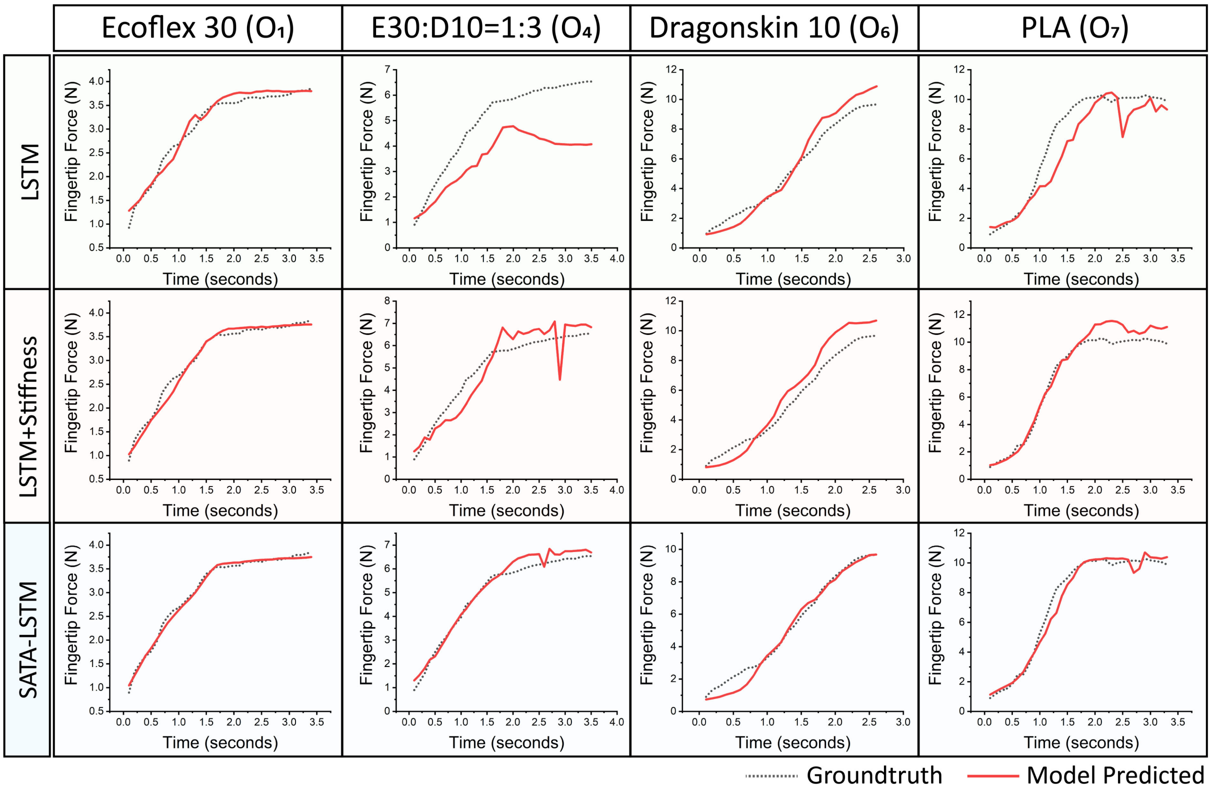

Fig. 5. Fingertip force estimation for objects of varying stiffness (567 N/m, 1433 N/m, 1967 N/m, Rigid) using LSTM, LSTM+Stiffness, and SATA-LSTM.

TABLE IV
FINGERTIP FORCE ESTIMATION RESULTS FOR EACH OBJECT

	O1	O2	O3	O4	O5	O6	O7
LR	1.58	1.49	1.22	1.26	1.00	1.66	2.69
RF	1.61	1.53	0.51	1.16	1.27	1.95	1.63
FC	1.22	0.59	0.61	0.92	1.36	1.01	2.87
LSTM	1.64	0.84	0.60	0.76	1.01	1.06	1.20
LSTM+S.	0.89	0.81	0.40	0.79	0.87	1.26	**0.75**
Ours	**0.62**	**0.59**	**0.37**	**0.62**	**0.81**	**1.01**	0.85

Measured in *RMSE* (N) LSTM+S. is abbreviation of LSTM+Stiffness

The performances of force estimation models that utilize predicted stiffness are compared in Table IV. Our model, SATA-LSTM, held the best performances for all deformable objects (O1–O6). SATA-LSTM achieved the lowest RMSE of 0.37 N for object O3 while the LSTM+Stiffness model yielded RMSE of 0.40 N for the same object. Both models yielded highest RMSE for O6, resulting in 1.26 N for LSTM+Stiffness and 1.01 N for SATA-LSTM. It can be noted that our algorithm outperformed the LSTM+Stiffness model in all stiffness ranges of tested deformable objects.

C. Effects of Sequence Lengths (T)

For our model to be used in real-time applications, it is important that the system can quickly estimate the applied fingertip forces. Therefore, we tested our model at various sequence lengths, which include T = 20, 40, and 60. All computations were performed using a single GPU (Titan RTX, NVIDIA, USA). For these sequence lengths, each fingertip force estimation required 0.0098 s, 0.0119 s, and 0.0159 s respectively. In terms of accuracy, the aforementioned time lengths yielded best RMSE of 0.837 N, 0.702 N, and 0.724 N. While the model performed faster at T = 20, the RMSE increased by 10% compared to when T = 40. Increasing the sequence length to T = 60 not only decreased the accuracy, but took 34% longer to make a single prediction compared to T = 40. Our current sequence length T = 40 captures the balance between high accuracy and high speed of algorithm.

D. Worst-Case Fingertip Force Estimation

Fig. 6(a) shows the cases in which the estimated fingertip forces differ from the ground truth by relatively large margin. When grasping the object made from Ecoflex-0050 (O2), the LSTM failed to predict the applied fingertip force. This is caused by the lack of stiffness information when estimating the applied forces. Despite incorporating the information about object's stiffness, the LSTM+Stiffness model and our SATA-LSTM model could not make accurate predictions. We assume that errors in stiffness regression resulted in inaccurate force estimation. Incorporating the attention mechanism to the stiffness estimation model may increase the accuracy of the predicted stiffness and improve the overall force estimation performance. Despite the discrepancies, it can be seen that compared to the other models, our proposed method still produced the estimations closest to the ground truth. This can be attributed to simultaneously training the stiffness estimation and the fingertip

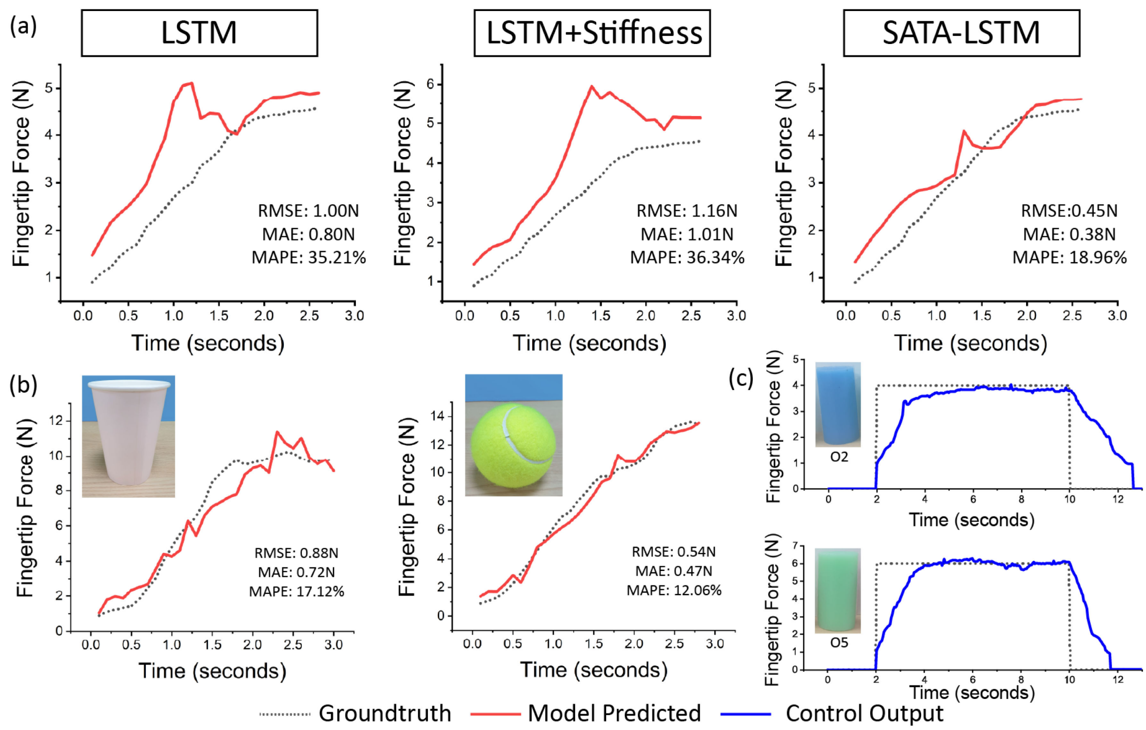

Fig. 6. (a) Worst case fingertip force estimation for LSTM, LSTM+Stiffness, and SATA-LSTM. (b) Estimating fingertip force applied to daily objects. It is noted that the daily objects were not used for training. (c) The force control of object O2(683 N/m) and object O5(1733 N/m) with target forces of 4 N and 6 N, respectively.

estimation model in SATA-LSTM. As a result, Fig. 6(a) shows that despite the errors in early stages, our model adjusted the stiffness estimation and caused the fingertip force predictions to move closer to the ground truth.

E. Feasibility on Untrained Daily Objects

To ensure the applicability of our method, we tested our model on some deformable objects that are commonly available. We evaluated different model's performances in estimating the fingertip forces applied to objects of relatively low and high stiffness : A letter cup (1215±24 N/m) and a tennis ball (4130±65 N/m). Fig. 6(b) shows the prediction results for both objects. Our model predicted the applied forces with RMSE of 0.880 N and 0.536 N for letter cup and tennis ball. We believe that the relatively large RMSE for the letter cup can be attributed to the sliding of the FSR sensor during grasping. The surface of the letter cup is much smoother in comparison to the silicone objects. Thus, when firmly grasping the letter cup, slipping between the FSR sensor and the contact surfaces would occur more frequently compared to grasping the silicone objects. However, our model still captured the overall trend of fingertip forces applied to deformable objects that it has not previously encountered.

F. Repeatability Test

We evaluated SATA-LSTM on a set of test data collected from a re-assembled actuation system to test the repeatability of our method. The test data was collected on a different day than when the training data was gathered. Table V shows that while the overall performances of models have decreased, our proposed method showed the least variance from the original results. For SATA-LSTM, the performance degraded in RMSE from 0.702 N to 0.805 N, MAE from 0.462 N to 0.639 N, and MAPE from 11.3% to 16.6%. Other methods showed more severe degradation. For LSTM+Stiffness, RMSE rose from 0.827 N to 1.139 N, MAE increased from 0.538 N to 0.851 N, and MAPE rose from 13.2% to 19.4%. For LSTM, which does not reflect the stiffness information, the RMSE, MAE, and MAPE all more than doubled the previously obtained results. The overall performance degradation can be attributed to alteration of the placement of the actuation system on the forearm. These effects can be alleviated by fine-tuning the model with additional data collected using the reassembled system.

TABLE V
FINGERTIP FORCE ESTIMATION RESULTS FOR REPEATABILITY

	RMSE (N)	*MAE* (N)	*MAPE* (%)
LSTM	2.501	1.604	47.7
LSTM+Stiffness	1.139	0.851	19.4
Ours	**0.805**	**0.639**	**16.6**

G. Real-Time Force Control

To test the real-time applicability of our method, we conducted real-time force control on objects of relatively low and high stiffness (O2 and O5). A PID controller was implemented to maintain the applied force at a target level for 8 seconds. The target forces were set to 80% of maximum grasping force applied to each object during data collection. Rounded to the nearest whole number, the target forces were 4 N and 6 N for O2 and O5 respectively. As shown in Fig. 6(c), for grasping O2, it took about 1.8 seconds to reach 90% of 4 N target force. After this period, our system maintains the applied force at the target level with RMSE of 0.211 N and MAPE of 5.1%. For O5, it took 1.6 seconds to reach 90% of the 6 N target force. After this period, the force is controlled at the target level with RMSE 0.161 N and MAPE 2.1%. Our control mechanism for soft objects was subject to deformation, which caused delays in reaching the target force level. However, after reaching the target force, applied force was controlled at an average MAPE of 3.6%, performing comparable result to the study done by Kang *et al.* [10] (3.69% MAPE).

V. Discussion and Conclusion

A deep-learning based model that can predict the fingertip force applied to deformable objects is proposed in this letter. The model uses data from actuation system, which include motor encoder values, motor current, and wire tension. In order to test our method, we developed NAME-TAG, a portable wearable robotic glove featuring a TSM-incorporated actuation system that can be worn on the forearm. Estimating the fingertip force applied to deformable objects is challenging due to varying non-linearity and hysteresis caused by objects' stiffness. The SATA-LSTM model, which integrates the estimated stiffness model with the fingertip force estimation model, aimed to resolve the aforementioned issues. The performance of our model was evaluated by comparing it to five learning-based models. To examine our model's general applicability, fingertip forces were estimated for grasping of deformable objects found in daily life: a letter cup and a tennis ball and real-time force control was performed.

Our proposed model, SATA-LSTM, accurately estimated the applied fingertip forces for objects of varying stiffness and outperformed three compared models. It also successfully predicted the forces applied to untrained daily objects and controlled the amount of force applied to relatively soft and hard objects. This showed that incorporating objects' stiffness is a key factor in determining the forces being applied to deformable objects. SATA-LSTM mitigates the effects of non-linearity by simultaneously training the stiffness estimation and fingertip force estimation model, and applying the stiffness information to the inputs and hidden layers of force estimation model.

Future works could be extended to incorporating our model with the intention detection methods discussed in [8]. Upon detecting the user's intent to grasp deformable objects, our model would be utilized to provide the fingertip force information to the force control algorithm. This would enable the wearable robotic glove to apply appropriate forces to the various objects that the user interacts with. Thus, it could aid the user to grasp and use soft objects such as takeout coffee or toothpaste.

References

[1] H. In, B. B. Kang, M. Sin, and K.-J. Cho, "Exo-glove: A wearable robot for the hand with a soft tendon routing system," *IEEE Robot. Automat. Mag.*, vol. 22, no. 1, pp. 97–105, Mar. 2015.

[2] D. Popov, I. Gaponov, and J.-H. Ryu, "Portable exoskeleton glove with soft structure for hand assistance in activities of daily living," *IEEE/ASME Trans. Mechatronics*, vol. 22, no. 2, pp. 865–875, Apr. 2017.

[3] B. B. Kang, H. Lee, H. In, U. Jeong, J. Chung, and K.-J. Cho, "Development of a polymer-based tendon-driven wearable robotic hand," in *Proc. IEEE Int. Conf. Robot. Automat.*, 2016, pp. 3750–3755.

[4] C. J. Nycz, T. Bützer, O. Lambercy, J. Arata, G. S. Fischer, and R. Gassert, "Design and characterization of a lightweight and fully portable remote actuation system for use with a hand exoskeleton," *IEEE Robot. Automat. Lett.*, vol. 1, no. 2, pp. 976–983, Jul. 2016.

[5] B. B. Kang, H. Choi, H. Lee, and K.-J. Cho, "Exo-glove poly II: A polymer-based soft wearable robot for the hand with a tendon-driven actuation system," *Soft Robot.*, vol. 6, no. 2, pp. 214–227, 2019.

[6] L. Gerez, J. Chen, and M. Liarokapis, "On the development of adaptive, tendon-driven, wearable exo-gloves for grasping capabilities enhancement," *IEEE Robot. Automat. Lett.*, vol. 4, no. 2, pp. 422–429, Apr. 2019.

[7] A. Dwivedi, L. Gerez, W. Hasan, C.-H. Yang, and M. Liarokapis, "A soft exoglove equipped with a wearable muscle-machine interface based on forcemyography and electromyography," *IEEE Robot. Automat. Lett.*, vol. 4, no. 4, pp. 3240–3246, Oct. 2019.

[8] D. Kim *et al.*, "Eyes are faster than hands: A soft wearable robot learns user intention from the egocentric view," *Sci. Robot.*, vol. 4, no. 26, 2019, Art. no. eaav2949.

[9] P. Tran, S. Jeong, S. L. Wolf, and J. P. Desai, "Patient-specific, voice-controlled, robotic FLEXotendon glove-II system for spinal cord injury," *IEEE Robot. Automat. Lett.*, vol. 5, no. 2, pp. 898–905, Apr. 2020.

[10] B. B. Kang *et al.*, "Learning-based fingertip force estimation for soft wearable hand robot with tendon-sheath mechanism," *IEEE Robot. Automat. Lett.*, vol. 5, no. 2, pp. 946–953, Apr. 2020.

[11] B. Kim, J. Ryu, and K.-J. Cho, "Joint angle estimation of a tendon-driven soft wearable robot through a tension and stroke measurement," *Sensors*, vol. 20, no. 10, p. 2852, 2020.

[12] X. Li, L. Cao, A. M. H. Tiong, P. T. Phan, and S. J. Phee, "Distal-end force prediction of tendon-sheath mechanisms for flexible endoscopic surgical robots using deep learning," *Mechanism Mach. Theory*, vol. 134, pp. 323–337, 2019.

[13] D. Kim *et al.*, "Review of machine learning methods in soft robotrics," *PLoS ONE*, vol. 16, no. 2, pp. 1–24, 2021, Art. no. e0246102.

[14] S. Hochreiter and J. Schmidhuber, "Long short-term memory," *Neural Comput.*, vol. 9, no. 8, pp. 1735–1780, 1997.

[15] S. Han, T. Kim, D. Kim, Y.-L. Park, and S. Jo, "Use of deep learning for characterization of microfluidic soft sensors," *IEEE Robot. Automat. Lett.*, vol. 3, no. 2, pp. 873–880, Apr. 2018.

[16] T. G. Thurutel, B. Shih, C. Laschi, and M. T. Tolley, "Soft robot perception using embedded soft sensors and recurrent neural networks," *Sci. Robot.*, vol. 4, no. 26, 2019, Art. no. eeav1488.

[17] S. Cheon *et al.*, "Single EMG sensor-driven robotic glove control for reliable augmentation of power grasping," *IEEE Trans. Med. Robot. Bionics*, vol. 3, no. 1, pp. 179–189, Feb. 2021.

[18] H. U. Whitesides Group, "Pneunets bending actuators," Softroboticstoolkit.com. https://softroboticstoolkit.com/book/pneunets-bending-actuator. (accessed Dec. 1, 2020).

[19] G. De Pasquale, L. Mastrototaro, L. Pia, and D. Burin, "Wearable system with embedded force sensors for neurologic rehabilitation trainings," in *Proc. Symp. Des., Test, Integration Packag. MEMS MOEMS*, 2018, pp. 1–4.

[20] I. Goodfellow, Y. Bengio, A. Courville, and Y. Bengio, *Deep Learning*, vol. 1, p.418–422. Cambridge, MA, USA: MIT press, 2016.

[21] C. Si, W. Chen, W. Wang, L. Wang, and T. Tan, "An attention enhanced graph convolutional LSTM network for skeleton-based action recognition," in *Proc. IEEE/CVF Conf. Comput. Vis. Pattern Recognit.*, 2019, pp. 1227–1236.

[22] A. Vaswani *et al.*, "Attention is all you need," in *Proc. Adv. Neural Inf. Process. Syst.*, I. Guyon, U. V. Luxburg, S. Bengio, H. Wallach, R. Fergus, S. Vishwanathan, and R. Garnett, eds. , Curran Assoc., 2017, vol. 30, pp. 5998–6008.